

## PROBING THE EPOCH OF REIONIZATION WITH THE LYMAN ALPHA FOREST AT $Z \sim 4 - 5$

RENYUE CEN<sup>1</sup>, PATRICK McDONALD<sup>2</sup>, HY TRAC<sup>3</sup>, & ABRAHAM LOEB<sup>3</sup>

<sup>1</sup> *Department of Astrophysical Sciences, Princeton University, Princeton, NJ 08544, USA* <sup>2</sup> *Canadian Institute for Theoretical Astrophysics, University of Toronto, Toronto, ON M5S 3H8, Canada* <sup>3</sup> *Harvard-Smithsonian Center for Astrophysics, Cambridge, MA 02138, USA*

*Draft version November 29, 2021*

### ABSTRACT

The inhomogeneous cosmological reionization process leaves tangible imprints in the intergalactic medium down to  $z \sim 4 - 5$ . The Lyman- $\alpha$  forest flux power spectrum provides a potentially powerful probe of the epoch of reionization. With the existing SDSS I/II quasar sample we show that two cosmological reionization scenarios, one completing reionization at  $z = 6$  and the other at  $z = 9$ , can be distinguished at  $\sim 7\sigma$  level by utilizing Ly $\alpha$  forest absorption spectra at  $z = 4.5 \pm 0.5$ , in the absence of other physical processes that may also affect the Ly $\alpha$  flux power spectrum. The redshift range  $z = 4 - 5$  may provide the best window, because there is still enough transmitted flux and quasars to measure precise statistics of the flux fluctuations, and the IGM still retains a significant amount of memory of reionization.

*Subject headings:*

### 1. INTRODUCTION

The history of cosmological reionization is presently primarily constrained by the cosmic microwave background observations of WMAP (Wilkinson Microwave Anisotropy Probe) (Dunkley et al. 2009) and the SDSS (Sloan Digital Sky Survey) quasar absorption spectra. The former gives an integral constraint, strongly suggesting that cosmological reionization may well be underway at  $z \sim 12$ , while the latter provides a solid anchor point at  $z \sim 6$  when the universe became largely transparent to Lyman limit photons (e.g., Fan et al. 2001; Becker et al. 2001; Cen & McDonald 2002; Fan et al. 2006b). At  $z \geq 6.3$  the lower bound on the neutral hydrogen fraction,  $x$ , of the IGM provided by SDSS observations is, however, fairly loose at  $x \geq 0.01$ . Thus, exactly when most of the neutral hydrogen became reionized is yet unknown and there are many possible scenarios that could meet the current observational constraints (e.g., Barkana & Loeb 2001; Cen 2003; Haiman & Holder 2003; Fan et al. 2006a; Wyithe & Cen 2007; Becker et al. 2007).

The process of inhomogeneous cosmological reionization leaves quantifiable and significant imprints on the thermal evolution of the IGM (Trac et al. 2008). In this *Letter*, we show that the Ly $\alpha$  forest flux spectrum at moderate redshift  $z = 4.5 \pm 0.5$  sensitively depends on and hence provides a very powerful probe of the epoch of reionization.

### 2. REIONIZATION MODELS

We use a hybrid code to accurately compute the reionization process, which consists of a high-resolution N-body code, a shock-capturing TVD hydro code and a ray-tracing radiative transfer (of Lyman limit photons) code. The reader is referred to Trac et al. (2008) for more details. We use the best fit WMAP 5-year cosmological parameters:  $\Omega_m = 0.28$ ,  $\Omega_\Lambda = 0.72$ ,  $\Omega_b = 0.046$ ,  $h = 0.70$ ,  $\sigma_8 = 0.82$ , and  $n_s = 0.96$  (Komatsu et al. 2009). We use

29 billion dark matter particles on an effective mesh with  $11,520^3$  cells in a comoving box of  $100 h^{-1}\text{Mpc}$ , yielding a particle mass resolution of  $2.68 \times 10^6 h^{-1}M_\odot$  allowing us to resolve all atomic cooling dark matter halos. A total of  $N = 1536^3$  gas cells of size  $65\text{kpc}/h$  are used and we trace five frequency bins at  $> 13.6\text{ eV}$  with the ray-tracing code. The star formation rate is controlled by the halo formation history. We adjust the ionizing photon escape fraction to arrive at two models, where reionization is completed early ( $z \sim 9$ ) and late ( $z \sim 6$ ), respectively; note that the halo formation histories in the two models are identical.

### 3. RESULTS

Previous studies (e.g., Furlanetto et al. 2004; Iliev et al. 2006; Lee et al. 2008) have shown that the reionization process proceeds in an inside-out fashion, where regions around high density peaks get reionized first. H II regions initially surround isolated galaxies that formed in high density peaks. With time these H II regions expand and lower density (void) regions are eventually engulfed by the expanding H II regions stemming from high density peaks. Consequently, the redshift of reionization of each individual spatial point,  $z_{\text{reion}}$ , is highly correlated with the underlying large-scale density field, with the positive correlation extending down to scales  $\sim 1 h^{-1}\text{Mpc}$ , as we have shown earlier (Trac et al. 2008). Once an expanding region is photo-ionized and photo-heated, it would cool subsequently due to adiabatic expansion and other cooling processes (primarily Compton cooling at high redshift), countered by photoheating of residual recombining hydrogen atoms (on the time scale of recombination) (e.g., Theuns et al. 2002; Hui & Haiman 2003). As a result, the strong correlation between  $z_{\text{reion}}$  and the underlying large-scale density is manifested in a strong anti-correlation between the temperature and the underlying large-scale density field. Specifically, different

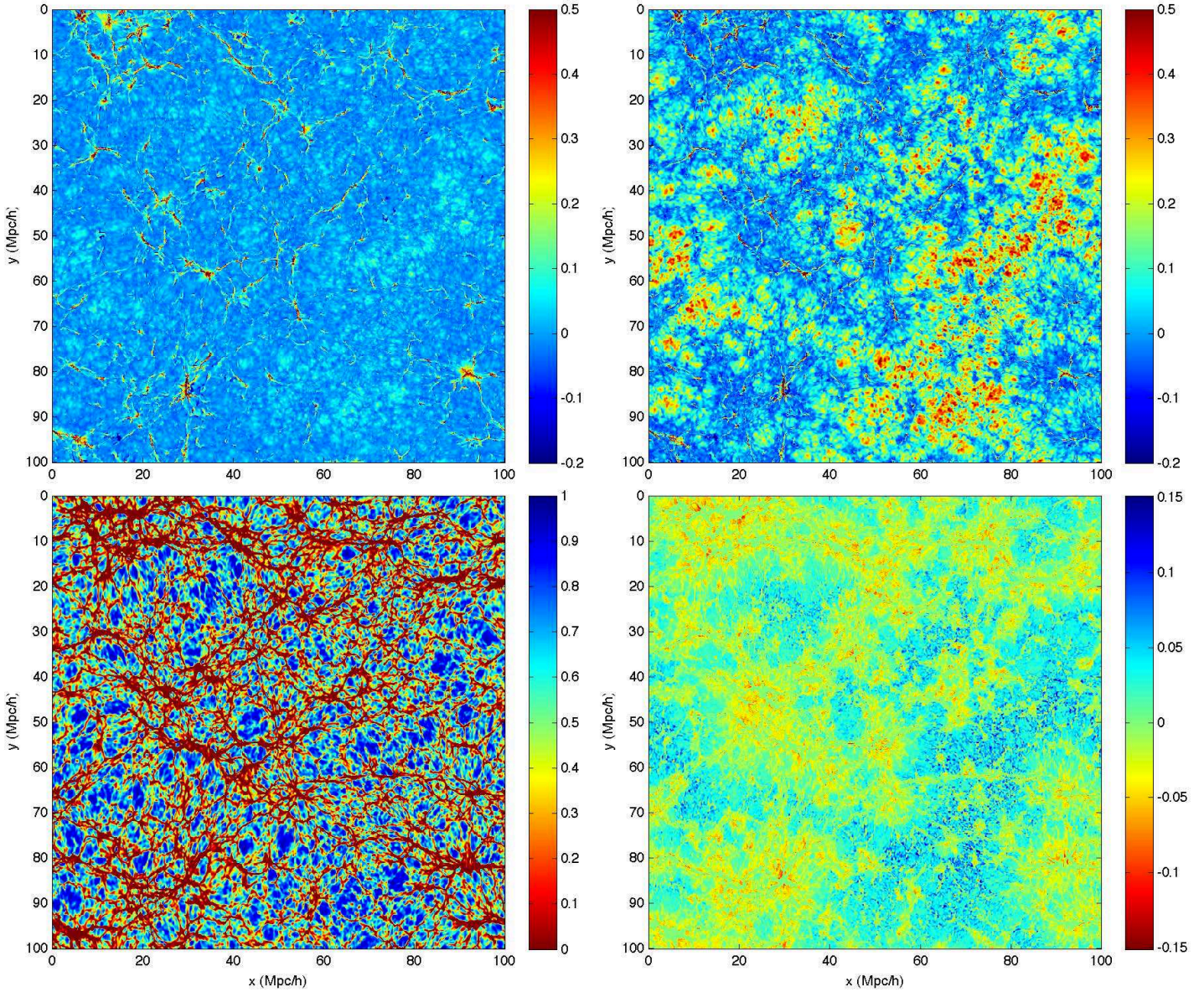


FIG. 1.— Top panels show the log of the ratio of gas temperature from the simulation to that prescribed by a fixed EoS at  $z = 4$ , for the early (left) and late (right) reionization model, respectively. We use EoS formula  $T = T_0(\rho/\rho_0)^{0.62}$ , where  $T_0$  is the temperature at mean density  $\rho_0$  in each model. The slice shown has a size  $(100 h^{-1}\text{Mpc})^2$  with a thickness equal to two hydro cells ( $130 h^{-1}\text{kpc}$ ). The distribution of flux transmission,  $F(\text{early}) = \exp(-\tau(\text{early}))$ , for the late reionization model is shown in the bottom left. The flux difference between the two models:  $F(\text{late}) - F(\text{early}) = \exp(-\tau(\text{late})) - \exp(-\tau(\text{early}))$  is shown in the bottom right panel.

regions of the same low densities  $\delta \leq$  a few (without large-scale smoothing in this case) would display a large, long-range-correlated, dispersion in temperature, immediately following the completion of reionization (e.g., Trac et al. 2008). (Note that virialized regions are not affected and do not retain any information of reionization in this regard.)

Both the anti-correlation between temperature and the underlying large-scale density and the consequent temperature dispersion at a fixed density weaken as time progresses and the temperature-density relation asymptotically approaches a so-called equation-of-state (EoS), a one-to-one mapping from IGM density to temperature (Hui & Gnedin 1997), with  $T = T_0(\rho/\rho_0)^{0.62}$  in the late-time limit. However, at the redshift range  $z = 4.5 \pm 0.5$ ,

the IGM has not had enough time to have completely relaxed to this state prescribed by the EoS such that quantitatively significant deviations from a deterministic EoS exist, if the universe was reionized, say, at  $z_{ri} \sim 6 - 8$ . The deviations from a simple temperature-density relation are larger for smaller  $z_{ri}$  at a given observed redshift.

In Fig. 1 we show the log of the ratio of gas temperature from the simulation to that prescribed by the asymptotic EoS at  $z = 4$  in a slice of size  $(100 h^{-1}\text{Mpc})^2$  with a thickness equal to two hydro cells ( $130 h^{-1}\text{kpc}$ ), for the early (top left panel) and late (top right panel) reionization model, respectively. The fields have been smoothed on cells of comoving length  $130 h^{-1}\text{kpc}$ . The small reddish/yellowish regions seen in the top left panel correspond to virialized regions, for which the plotted



ratio does not contain useful information. But these regions show clearly the location of ionizing sources. We see striking differences in temperature distributions between the two reionization models with respect to their respective asymptotic EoS values. In the early reionization model (top left panel) most of the regions have blue color (i.e., the ratio equal to  $\sim 1$ ) and appear to have mostly relaxed to the state predicted by the asymptotic EoS, while some low density regions in the voids still display yellowish color with a temperature that is higher than that of the asymptotic EoS by 30 – 50%. On the other hand, in the late reionization simulation (top right panel), while regions just outside the shock-heated filaments and halos (bluish color) have largely relaxed to the asymptotic EoS, regions of comparable local densities in the voids are much hotter than that of the asymptotic EoS, by a factor of 1.5 – 2.5.

Because the neutral hydrogen fraction in regions of moderate density is determined by the balance between photoionization rate and recombination rate, the latter of which is a function of temperature, the two different temperature distributions in the two reionization models result in different large-scale neutral hydrogen distribution. In the bottom left panel of Fig. 1 we show the expected flux transmission,  $F(\text{early}) = \exp(-\tau(\text{early}))$ , for the early reionization model, where  $\tau(\text{early})$  is the Ly $\alpha$  optical depth computed based on the distribution of neutral hydrogen density, gas peculiar velocity and temperature at  $z = 4$  in the early reionization model. In computing the neutral hydrogen fraction we have used a uniform background radiation field with its amplitude adjusted such that both models yield the same mean transmitted flux of  $\langle F \rangle = 0.43$  at  $z = 4$ , as observed (Fan et al. 2006b). In the bottom right panel the flux difference between the two models,  $F(\text{late}) - F(\text{early})$ , is shown, where it is clearly seen that the transmitted Ly $\alpha$  flux is significantly affected by the temperature difference at  $z = 4$ , resulting in fractional difference in the transmitted flux in the voids between the two models of  $\sim 15\%$  (blue regions). Specifically, there is more transmitted flux in the void regions in the late reionization model, compensated by comparably reduced transmitted flux in high density regions. It is noted that, at  $z \geq 4$ , the majority of transmitted Ly $\alpha$  flux comes from the lowest density regions of  $\delta \leq \text{a few}$ .

Fig. 2 shows the ratio of flux power spectrum in the late reionization model to that in the early reionization model at  $z = 4$  (black solid) and  $z = 5$  (black dashed). It appears that the large-scale anti-correlation between density and deviations from a single EoS in the late reionization model leads to a significant amount of extra power in the flux spectrum (specifically, relatively high temperatures in late-reionizing under-dense regions lead them to produce even less absorption than they otherwise would). The difference between the flux power spectra of the two reionization models increases with scale, reaching 20% at  $k = 0.001(\text{km/s})^{-1}$  at  $z = 4$ ; the difference is still larger at  $z = 5$  ( $\sim 30\%$ ), as expected, due to still larger difference in the temperature hence flux transmission between the two reionization models. The black error bars indicate the statistical errors expected with the full SDSS I/II sample (completed, but not yet fully analyzed). With

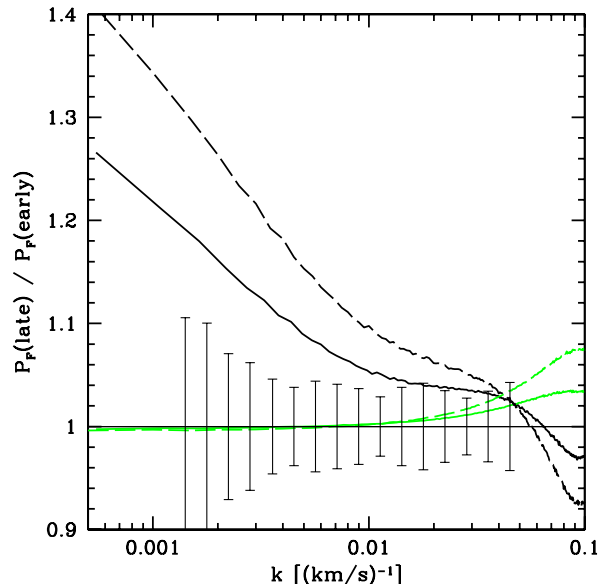


FIG. 2.— Black solid and dashed curves are the ratio of flux power spectrum in the late reionization model to that in the early reionization model at  $z = 4$  and  $z = 5$ , respectively. Also shown are the two green curves are the corresponding ratios produced by replacing the real temperature in each simulation by that prescribed by the EoS given density (the same EoS in both simulations). The black error bars are the error one can expect from the full SDSS I/II sample plus existing high resolution data. The error bars will be approximately uncorrelated. A formal analysis of the 16 data points indicates that the two reionization models can be differentiated at  $7\sigma$  level.

$z \sim 4$  SDSS I/II data plus existing high resolution data, one can distinguish formally between these two reionization models at  $7\sigma$  level. However, we note that the statistical differences between the two models are un-marginalized, i.e., not taking into account other physical effects that affect the Ly $\alpha$  flux power spectrum determination (e.g. McDonald et al. 2005). Therefore, the quoted statistical significance only serves as an indication of the potential power of this statistics.

For comparison, the corresponding flux power spectrum ratios at  $z = 4$  and  $z = 5$ , if both models follow the same EoS (given density), are shown (green curves) in Fig. 2. In this case, aside from the relatively small difference on small scales due to cumulative dynamical affects on the gas density by the difference in the gas pressure histories, the two models have identical flux power spectrum on large scales. This clearly demonstrates that the large difference in the flux power spectra between the two reionization models (black curves in Fig. 2) is a result of large differences in the contemporaneous temperature distributions.

#### 4. DISCUSSION

This effect of inhomogeneous reionization on the flux power spectrum was explored earlier by Lai et al. (2006) at  $z = 3$ , based on a semi-analytic model. Their focus is on  $z = 3$  and found that, on large scales,  $k \sim 0.001(\text{km/s})^{-1}$ , temperature fluctuations lead to an increase in the  $z \sim 3$  flux power spectrum by at most 10%. Our focus here is at higher redshifts  $z = 4 - 5$  and the effects, not surprisingly, are larger and potentially more

discriminating.

A fluctuating radiation background, produced largely by radiation from sparsely distributed quasars but also by galaxies, can affect the flux power spectrum (Meiksin & White 2004; Croft 2004; McDonald et al. 2005). Larger fluctuations in the radiation background give rise to larger amplitudes of the flux power spectrum at large scales (e.g. McDonald et al. 2005, Figures 6,7 therein). This enhancement of the flux power spectrum on large scales due to a fluctuating radiation background will be in addition to what is caused by the gas temperature fluctuations shown here, if QSOs were dominant. The radiation contribution from stars may be more dominant at the redshift range of concern here (e.g., Faucher-Giguere et al. 2009). Star formation is known to be biased and hence higher density regions, on average, tend to have higher radiation field than lower density regions. Thus, the two effects due to a fluctuating radiation background and an inhomogeneous reionization process may be partially degenerate or have a tendency to cancel each other's contribution, although there is a possibility that the radiation fluctuations may be relatively modest (e.g., Mesinger & Furlanetto 2009). A more careful modeling of the contribution from quasars as well as radiation sinks (such as Lyman limit systems) is required in a comprehensive modeling. The purpose of this *Letter* is to demonstrate that, if the effects on the Ly $\alpha$  flux power spectrum determination due to the epoch of reionization were the only relevant ones, then a precise measure of the flux power spectrum with the full SDSS I/II data will be able to place a very tight constraint on the epoch of reionization.

However, a detailed comparison between models and SDSS I/II observations requires a full analysis of all astrophysical/cosmological processes that may affect

the determination of the flux power spectrum and some of them may be degenerate to varying degrees (McDonald et al. 2005), including fluctuating radiation field, damped Ly $\alpha$  systems, galaxy formation feedback, initial photoheating temperature (i.e., related to IMF of high redshift galaxies), X-ray heating, He II reionization, among others, before its statistical potential can be precisely marginalized and quantified. We will perform such an analysis in a future study.

## 5. CONCLUSIONS

Utilizing state-of-the-art radiative transfer hydrodynamic simulations of cosmological reionization, we put forth the point that the inhomogeneous reionization process imprints important and quantitatively significant signatures in the intergalactic medium at  $z = 4.5 \pm 0.5$  that can be probed by the Ly $\alpha$  forest in the quasar absorption spectra. We illustrate that with Ly $\alpha$  forest data at  $z = 4 - 5$  to be provided by the SDSS I/II full data sample, one may be able to distinguish between two cosmological epochs of reionization, one at  $z = 6$  and the other  $z = 9$  at  $7\sigma$  level, if they were the only effects on the determination of the Ly $\alpha$  flux power spectrum.

We thank J. Chang at NASA for invaluable supercomputing support. This work is supported in part by NASA grants NNG06GI09G and NNX08AH31G. Computing resources were in part provided by the NASA High-End Computing (HEC) Program through the NASA Advanced Supercomputing (NAS) Division at Ames Research Center. PM acknowledges support of the Beatrice D. Tremaine Fellowship. HT is supported by an Institute for Theory and Computation Fellowship.

## REFERENCES

- Barkana, R., & Loeb, A. 2001, *Phys. Rep.*, 349, 125  
 Becker, G. D., Rauch, M., & Sargent, W. L. W. 2007, *ApJ*, 662, 72  
 Becker, R. H., Fan, X., White, R. L., Strauss, M. A., Narayanan, V. K., Lupton, R. H., Gunn, J. E., & Annis, J. 2001, *AJ*, 122, 2850  
 Cen, R. 2003, *ApJ*, 591, 12  
 Cen, R., & McDonald, P. 2002, *ApJ*, 570, 457  
 Croft, R. A. C. 2004, *ApJ*, 610, 642  
 Dunkley, J., Komatsu, E., Nolta, M. R., Spergel, D. N., Larson, D., Hinshaw, G., Page, L., Bennett, C. L., Gold, B., Jarosik, N., Weiland, J. L., Halpern, M., Hill, R. S., Kogut, A., Limon, M., Meyer, S. S., Tucker, G. S., Wollack, E., & Wright, E. L. 2009, *ApJS*, 180, 306  
 Fan, X., Carilli, C. L., & Keating, B. 2006a, *ARA&A*, 44, 415  
 Fan, X., Narayanan, V. K., Lupton, R. H., Strauss, M. A., Knapp, G. R., Becker, R. H., White, R. L., Pentericci, L., Leggett, S. K., Haiman, Z., Gunn, J. E., Ivezić, Ž., Schneider, D. P., Anderson, S. F., Brinkmann, J., Bahcall, N. A., Connolly, A. J., Csabai, I., Doi, M., Fukugita, M., Geballe, T., Grebel, E. K., Harbeck, D., Hennesy, G., Lamb, D. Q., Miknaitis, G., Munn, J. A., Nichol, R., Okamura, S., Pier, J. R., Prada, F., Richards, G. T., Szalay, A., & York, D. G. 2001, *AJ*, 122, 2833  
 Fan, X., Strauss, M. A., Becker, R. H., White, R. L., Gunn, J. E., Knapp, G. R., Richards, G. T., Schneider, D. P., Brinkmann, J., & Fukugita, M. 2006b, *AJ*, 132, 117  
 Faucher-Giguere, C., Lidz, A., Zaldarriaga, M., & Hernquist, L. 2009, *ArXiv e-prints*  
 Furlanetto, S. R., Zaldarriaga, M., & Hernquist, L. 2004, *ApJ*, 613, 1  
 Haiman, Z., & Holder, G. P. 2003, *ApJ*, 595, 1  
 Hui, L., & Gnedin, N. Y. 1997, *MNRAS*, 292, 27  
 Hui, L., & Haiman, Z. 2003, *ApJ*, 596, 9  
 Iliev, I. T., Mellema, G., Pen, U.-L., Merz, H., Shapiro, P. R., & Alvarez, M. A. 2006, *MNRAS*, 369, 1625  
 Komatsu, E., Dunkley, J., Nolta, M. R., Bennett, C. L., Gold, B., Hinshaw, G., Jarosik, N., Larson, D., Limon, M., Page, L., Spergel, D. N., Halpern, M., Hill, R. S., Kogut, A., Meyer, S. S., Tucker, G. S., Weiland, J. L., Wollack, E., & Wright, E. L. 2009, *ApJS*, 180, 330  
 Lai, K., Lidz, A., Hernquist, L., & Zaldarriaga, M. 2006, *ApJ*, 644, 61  
 Lee, K.-G., Cen, R., Gott, J. R. I., & Trac, H. 2008, *ApJ*, 675, 8  
 McDonald, P., Seljak, U., Cen, R., Bode, P., & Ostriker, J. P. 2005, *MNRAS*, 360, 1471  
 Meiksin, A., & White, M. 2004, *MNRAS*, 350, 1107  
 Mesinger, A., & Furlanetto, S. 2009, *ArXiv e-prints*  
 Theuns, T., Schaye, J., Zaroubi, S., Kim, T.-S., Tzanavaris, P., & Carswell, B. 2002, *ApJ*, 567, L103  
 Trac, H., Cen, R., & Loeb, A. 2008, *ApJ*, 689, L81  
 Wyithe, J. S. B., & Cen, R. 2007, *ApJ*, 659, 890